JOURNAL OF RHEOLOGY

Obtaining reliable transient rheological data on concentrated short fiber suspensions using a rotational rheometer

Aaron P. R. Eberle, Donald G. Baird, Peter Wapperom, and Gregorio M. Vélez-García

Citation: Journal of Rheology (1978-present) **53**, 1049 (2009); doi: 10.1122/1.3177348
View online: http://dx.doi.org/10.1122/1.3177348
View Table of Contents: http://scitation.aip.org/content/sor/journal/jor2/53/5?ver=pdfcov
Published by the The Society of Rheology

Obtaining reliable transient rheological data on concentrated short fiber suspensions using a rotational rheometer

Aaron P. R. Eberle and Donald G. Baird[a)]

Department of Chemical Engineering, Virginia Tech, Blacksburg, Virginia 24061

Peter Wapperom

Department of Mathematics, Virginia Tech, Blacksburg, Virginia 24061

Gregorio M. Vélez-García

Department of Macromolecular Science and Engineering, Virginia Tech, Blacksburg, Virginia 24061

(Received 28 July 2008; final revision received 24 June 2009)

Synopsis

The conventional method for obtaining transient rheological data on short glass fiber-filled polymeric fluids is to use the parallel disk (PP) geometry in a rotational rheometer. Using the PP geometry large transient stress overshoot behavior was observed during the startup of flow measurements on a 30 wt % short glass fiber-filled polybutylene terephthalate. A contributing factor to this behavior is believed to be induced fiber collisions caused by the inhomogeneous velocity field (radial varying velocity gradient). A novel approach was taken in which a "donut" shaped sample was used in a cone-and-plate device (CP-D) to maintain a sufficient gap to fiber length ratio. The magnitude of the first normal stress difference was reduced by 70%, and the time to reach steady state was reduced by 100 strain units. The Lipscomb model coupled with the Folgar–Tucker model for the evolution of fiber orientation was fit to the stress growth behavior measured using both the PP geometry and CP-D resulting in different parameters. In addition, the fitted model parameters were found to depend on the initial fiber orientation. It is believed that the CP-D allows for an accurate determination of the stress growth behavior and eventually will allow one to obtain unambiguous model parameters.
 [DOI: 10.1122/1.3177348]

I. INTRODUCTION

The physical properties of parts manufactured by means of injection or compression molding of short glass fiber composites significantly depends on the orientation of the fibers generated during mold filling. As a result, it is desired to accurately predict fiber orientation as a function of mold design and composite rheological properties. Hence, the rheological behavior of these materials and its connection to fiber orientation as deter-

[a)]Author to whom correspondence should be addressed; electronic mail: dbaird@vt.edu

mined in simple shear flow are of significant relevance to the development of stress and orientation relations that can accurately predict fiber orientation in complex flow situations.

The rheological behavior of suspensions containing short glass fibers is complex because it not only depends on the suspending medium but on the fiber characteristics (i.e., concentration, aspect ratio, and orientation). The dynamic behavior of the fiber is dependent on the degree interaction, i.e., hydrodynamic and/or direct contact. As a result, it is common to classify fiber suspensions into three concentration régimes based on excluded volume defined through the fiber volume fraction ϕ and aspect ratio a_r of the fiber: dilute ($\phi \ll a_r^{-2}$), semidilute ($a_r^{-2} \ll \phi \ll a_r^{-1}$), and concentrated ($\phi > a_r^{-1}$) [Doi and Edwards (1988)]. Typically, the aspect ratio of short glass fiber lies in the range $15 < a_r < 100$ and composites of industrial interest typically have fiber concentrations $\phi > 0.1$, which places the materials of interest in the concentrated régime [Advani and Sozer (2003)].

Characterizing the rheological behavior of composite melts containing glass fibers has proven to be a formidable task. To prevent wall effects on the dynamic behavior of the fiber, Blakeney (1966) suggested that the rheometer gap be greater than three times the fiber length L. In rotational rheometers, cone-and-plate (CP) fixtures impose a homogeneous velocity field, but the gap height varies linearly from the center ($\sim 50\ \mu$m) to the plate rim. At the center of the plates where the rheometer gap is small compared to the fiber length, the excessive fiber-boundary interaction can cause a suppression of the transient behavior [Utracki (1991)]. As a result, it is common practice for researchers to use the parallel disk (PP) geometry in rotational rheometers to perform the rheological measurements as it allows for a certain amount of gap control. However, in the PP fixtures, the tangential velocity at any point on the moving plate is a function of the radial position [Bird *et al.* (1987)]. This results in an inhomogeneous velocity field. Both experimental [Iso *et al.* (1996); Moses *et al.* (2001)] and theoretical [Barbosa and Bibbo (2000)] results have shown that for dilute and semidilute suspensions of fibers where external forces, inter-particle contact, and hydrodynamic forces are neglected, the rate of change in the particle orientation is a function of the velocity gradient [Moses *et al.* (2001)]. For concentrated suspensions where the inter-particle spacing can be on the order of the fiber diameter, we believe that the inhomogeneous velocity field may induce excessive fiber contact resulting in a misleading measurement of the suspension's time dependent stress response to deformation.

Many researchers have studied the experimental stress growth behavior of non-dilute suspensions of short glass fibers. A good summary of some of these works can be found in Laun (1984), Ganani and Powell (1985), Powell (1990), Zirnsak *et al.* (1994), Sepehr *et al.* (2004c), and Eberle *et al.* (2008). From these works, it can be shown that in general, as the concentration and/or aspect ratio of the fiber increases, the overshoot behavior of the shear stress growth coefficient η^+ and first normal stress difference growth function N_1^+ increases. The overshoot is attributed to a reorientation of the fibers as they try to establish an orientation along the fluid streamlines, which is the orientation of the least resistance to flow.

Current fiber-suspension theories used to predict the stress growth behavior depend on the ability to account for the relationship between the dynamic behavior of the fiber microstructure (average orientation) and the macroscopic rheological properties [Dinh and Armstrong (1984); Lipscomb *et al.* (1988); Sepehr *et al.* (2004a, 2004b)]. The result is a stress tensor describing the contribution from the presence of the fiber as a result of the hydrodynamic drag that is coupled to an equation describing the temporal evolution of the fiber orientation. Currently, there is no theory for concentrated suspensions; but it is a common practice in the literature to use the dilute or semidilute suspension theories

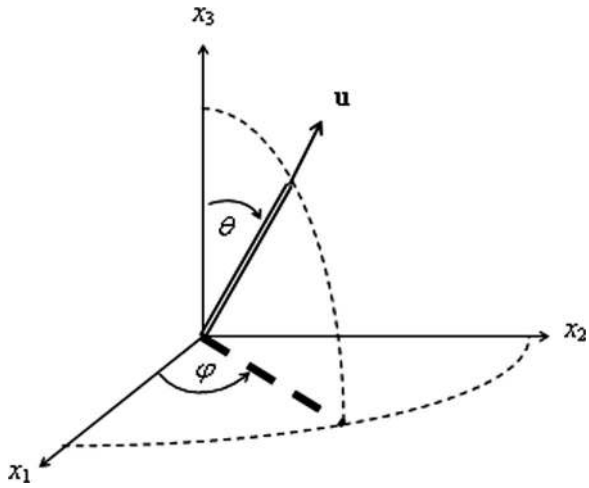

FIG. 1. Unit vector **u** describing the orientation state of a rigid fiber in spherical coordinates.

of Lipscomb *et al.* (1988), Dinh and Armstrong (1984), Shaqfeh and Fredrickson (1990), or Phan-Thien and Graham (1991) to simulate the rheology of concentrated suspensions. These theories give a fundamental approach to calculating the model parameters associated with magnitude of the hydrodynamic stress as a function of the fiber concentration and/or aspect ratio. However, Sepehr *et al.* (2004a, 2004b) were only able to accurately predict the rheological behavior of a concentrated short glass fiber-filled polymer melt when model parameters were fit to stress growth measurements. This suggests that the model parameters may be determined for a specific composite fluid with knowledge of the stress growth behavior. To obtain accurate parameters by fitting, one must first have an accurate measure of the transient stresses that truly represents the stress response to deformation of a fluid in a well defined flow field.

The purpose of this paper is to present a method to obtain reliable transient rheological data for suspensions containing short glass fibers using a rotational rheometer that could be used to obtain fitted unambiguous model parameters. First, we present experimental results of the stress growth behavior measured using the PP geometry as a function of gap height for a 30 wt % short glass fiber-filled polybutylene terephthalate (PBT-30), a matrix that behaves similarly to a Newtonian fluid. Measurements performed using the PP geometry are then compared to measurements performed using a novel technique, in which a "donut" shape sample is used in a CP device (CP-D) geometry to maintain a sufficient gap to fiber length ratio. Second, the Lipscomb model for stress coupled with the Folgar–Tucker model for orientation is fit to the transient stress growth behavior. The effects of the initial conditions and the model parameters determined from fitting stress growth data measured using the PP geometry and the CP-D are discussed.

II. THEORY

A. Orientation tensors

The orientation of a single fiber can be described with a unit vector **u** along the fiber axis as shown in Fig. 1. The average orientation of a large number of fibers of similar length can be described using a distribution function $\psi(\mathbf{u},t)$. A widely used and compact

way to represent the average orientation state is with the second- and fourth-order orientation tensors, which are defined as the second- and fourth-moments of the orientation distribution function [Advani and Tucker (1987)],

$$\mathbf{A}(t) = \int \mathbf{uu}\psi(\mathbf{u},t)d\mathbf{u}, \tag{1}$$

$$\mathbf{A}_4(t) = \int \mathbf{uuuu}\psi(\mathbf{u},t)d\mathbf{u}. \tag{2}$$

The trace of $\mathbf{A}$ is always equal to 1 and for a completely random orientation state $\mathbf{A} = 1/3\mathbf{I}$, where $\mathbf{I}$ is the unity tensor. In the limit that all the fibers are perfectly aligned in the x_1 direction, the only nonzero component is $A_{11}=1$.

B. Evolution of fiber orientation

The first theoretical work describing the evolution of high aspect ratio particle orientation that is easily extendable to rigid rods is that of Jeffery [Jeffery (1922)]. Jeffery extended Einstein's [Einstein (1906)] approach to solving the equations of motion for the flow of a Newtonian fluid around a spherical particle to that of a neutrally buoyant ellipsoidal particle in the absence of Brownian motion. The generalized Jeffery equation for the evolution of the vector $\mathbf{u}$ can be written as [Hand (1961); Giesekus (1962a, 1962b)]

$$\dot{\mathbf{u}} = \frac{D\mathbf{u}}{Dt} = \mathbf{W}\cdot\mathbf{u} + \lambda[\mathbf{D}\cdot\mathbf{u} - \mathbf{u}(\mathbf{u}\cdot\mathbf{D}\cdot\mathbf{u})], \tag{3}$$

where D/Dt is the material derivative, λ is a constant describing the ellipticity of the particle, $\mathbf{W}=[(\nabla\boldsymbol{v})^t-\nabla\boldsymbol{v}]/2$ is the vorticity, $\mathbf{D}=[\nabla\boldsymbol{v}+(\nabla\boldsymbol{v})^t]/2$ is the rate of strain tensor and, $\nabla\boldsymbol{v}=\partial v_j/\partial x_i$. For fibers, it is common to assume $\lambda\to 1$, which corresponds to a fiber with an infinitely large a_r. Using this approximation, Eq. (3) can be solved analytically for two equations describing the motion of the fiber in terms of the spherical angles φ and θ defined in Fig. 1 as [Barbosa and Bibbo (2000)]

$$\tan\,\theta(t) = \tan\,\theta_o[(\dot{\gamma}t)^2\,\sin^2\,\varphi_o + 2\dot{\gamma}t\,\sin\,\varphi_o\,\cos\,\varphi_o + 1]^{1/2}, \tag{4}$$

$$\tan\,\varphi(t) = \frac{1}{\cot(\varphi_o) + \dot{\gamma}t}, \tag{5}$$

where φ_o and θ_o are initial conditions. Both $\theta(t)$ and $\varphi(t)$ are functions of time and shear rate $\dot{\gamma}$ (the scalar magnitude of $\mathbf{D}$) or strain $\gamma=\dot{\gamma}t$. For non-dilute suspensions, Folgar and Tucker (1984) modified Eq. (3) to include a phenomenological term to account for fiber interaction. The Folgar–Tucker model can be written in terms of $\mathbf{A}$ for $\lambda\to 1$ as follows [Advani and Tucker (1987)]:

$$\frac{D\mathbf{A}}{Dt} = (\mathbf{W}\cdot\mathbf{A} - \mathbf{A}\cdot\mathbf{W}) + (\mathbf{D}\cdot\mathbf{A} + \mathbf{A}\cdot\mathbf{D} - 2\mathbf{D}{:}\mathbf{A}_4) + 2C_I\dot{\gamma}(\mathbf{I} - 3\mathbf{A}), \tag{6}$$

where C_I is a phenomenological parameter.

C. Stress

Lipscomb *et al.* (1988) proposed a stress equation for a suspension of high aspect ratio particles following the work of Hand (1961) and Giesekus (1962a, 1962b) as

$$\boldsymbol{\sigma} = -P\mathbf{I} + 2\eta_s\mathbf{D} + 2c_1\varphi\eta_s\mathbf{D} + 2\varphi\eta_s N\mathbf{D}:\mathbf{A}_4, \tag{7}$$

where $\boldsymbol{\sigma}$ is the total stress, c_1 is a constant, η_s is the suspending medium viscosity, and N is a dimensionless parameter that represents the coupling between the hydrodynamic stress contribution and the fiber orientation. Lipscomb *et al.* (1988) gave $c_1=2$ and N to be a function of the particle aspect ratio. Other theories of a similar form such as Dinh and Armstrong (1984), Shaqfeh and Fredrickson (1990), or Phan-Thien and Graham (1991) gave N to be a function of the fiber length, fiber diameter, number of fibers, and the average spacing between the fibers. However, N is frequently used as a fitting parameter, which is the approach we use in this work.

For the predicted material functions η^+ and N_1^+ in which the velocity field is homogeneous, we use the superscript notation CP to refer to the homogeneous velocity field found in the CP geometry. η^{CP} and N_1^{CP} for simple shear flow kinematics ($v_1=\dot{\gamma}y$ and $v_2=v_3=0$) can be written as

$$\eta^{\mathrm{CP}} = \sigma_{12}/\dot{\gamma} = \eta_s + c_1\eta_s\varphi + 2\eta_s\varphi N A_{1212}, \tag{8}$$

$$N_1^{\mathrm{CP}} = 2\varphi\eta_s\dot{\gamma}N(A_{1211} - A_{1222}). \tag{9}$$

This is in contrast to the equations used to predict the material functions in which the velocity field is inhomogeneous. In the case of an inhomogeneous velocity field, as in PP rheometers, the shear strain, and hence, average fiber orientation varies with radial position. The material functions η^+ and N_1^+–N_2^+ in this case are denoted by the superscript PP and have the form

$$\eta^{\mathrm{PP}} = \sigma_{12}/\dot{\gamma}_R = \eta_s + c_1\varphi\eta_s + \frac{8\varphi\eta_s N}{\gamma_R^4}\int_0^{\gamma_R} A_{1212}\gamma^3 d\gamma, \tag{10}$$

$$N_1^{\mathrm{PP}} - N_2^{\mathrm{PP}} = \frac{6\eta_s\varphi N\dot{\gamma}_R}{\gamma_R^3}\int_0^{\gamma_R}(A_{1211} - 2A_{1222} + A_{1233})\gamma^2 d\gamma. \tag{11}$$

III. EXPERIMENTAL

A. Materials

For this work, a commercially available 30 wt % (volume fraction $\phi=0.1766$) short glass fiber-filled PBT-30 produced by GE Plastics under the trade name Valox 420 was used. Linear viscoelastic measurements confirmed that the matrix exhibits little complex viscosity dependence on frequency and a small storage modulus [Eberle (2008)]. To examine the effect of fiber concentration on the rheological behavior, PBT-30 was diluted to concentrations of 4.07, 8.42, 15, 20, and 25 wt %. Compounding was accomplished by passing dry blended amounts of PBT-30 and the neat matrix through the extruder section of an Arburg Alrounder 221-55-250 injection molder at a rpm of 200. The extrudate was collected before entering the runner of the mold and pelletized. The pellets were then compression molded for rheological testing to PP and CP geometries at 260 °C. Precautions were taken to minimize the degree of thermo-oxidative degradation of the PBT matrix by drying the materials at 120 °C for a minimum of 12 h in a vacuum oven at a pressure smaller than 0.4 in. Hg before sample extrusion, molding, or testing [Botelho *et al.* (2001)]. The PBT-30 was also subjected to the same extrusion conditions to maintain a consistent shear and thermal history on all samples.

To characterize the glass fiber within the suspension, pyrolysis was performed on the PBT-30 pellets after extrusion at 500 °C to separate the fibers from the matrix. The fiber length was determined by randomly measuring the length of 1000 fibers. The number average and weight average fiber length of PBT-30 was found to be $L_n = 0.3640$ and $L_w = 0.4388$ mm, respectively. The same fiber length measurement was performed on all the diluted concentrations and was found to be within $0.3640 \leq L_n \leq 0.3740$ and $0.4388 \leq L_w \leq 0.4578$ mm. The fiber diameter D was determined directly from images taken of fiber cross sections using a confocal laser microscope, discussed later, and the average diameter of 1000 fibers was found to be $D = 12.9$ μm. This relates to a number average aspect ratio for PBT-30 of $a_r \cong 28.2$. The glass fibers within the suspension can be considered non-Brownian as the Peclet number (Pe) was approximately 10^{13} [Larson (1999)].

B. Rheological measurements

All rheological measurements were performed on a Rheometrics Mechanical Spectrometer (RMS-800) at 260 °C in a nitrogen environment with a freshly loaded preformed sample. Two sample geometries were used: a 25 mm diameter PP and a 50 mm diameter CP, with a 0.1 rad cone angle. In the results and discussion section, each measurement is discussed with relation to the geometry used to perform the measurement.

In this work, we are primarily interested in the transient rheological behavior at the startup of shear flow. For measurements performed using the PP fixtures, η^+ and $N_1^+ - N_2^+$ were calculated as functions of torque $M(t)$ and normal force $F(t)$ as follows [Macosko (1994)]:

$$\eta^+(t) = \frac{M(t)}{2\pi R^3 \dot{\gamma}_R}\left(3 + \frac{d \ln M}{d \ln \dot{\gamma}_R}\right), \tag{12}$$

and

$$N_1^+(t) - N_2^+(t) = \frac{F_z(t)}{\pi R^2 \dot{\gamma}_R}\left(2 + \frac{d \ln F_z}{d \ln \dot{\gamma}_R}\right), \tag{13}$$

where R is the radius of the plate and $\dot{\gamma}_R$ is the shear rate at R. The derivatives $(d \ln M / d \ln \dot{\gamma}_R)$ and $(d \ln M / d \ln \dot{\gamma}_R)$ in Eqs. (12) and (13), respectively, where estimated graphically over the entire range of $\dot{\gamma}_R$ presented.

Measurements with the CP geometry were performed with two different samples. Disks compression molded to the specifications for the geometry gap and modified CP sample disks, which we refer to as donut samples. The donut samples were produced by taking preformed disks and boring a hole through the center. A schematic drawing of the donut sample can be found in Fig. 2 and is discussed later. Using the CP fixtures, the measured material functions η^+ and N_1^+ were calculated from the following equations modified from Macosko (1994):

$$\eta^+(t) = \frac{3M(t)}{2\pi\dot{\gamma}}(R_o^3 - R_i^3)^{-1}, \tag{14}$$

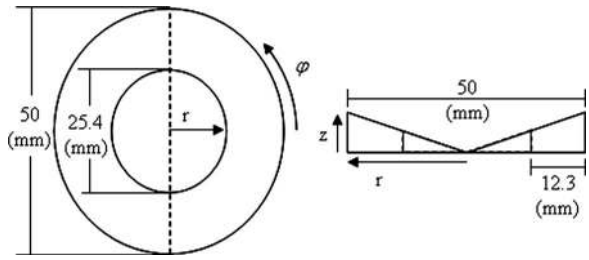

FIG. 2. Schematic drawing and cross-sectional profile of the donut sample.

$$N_1^+(t) = \frac{2F_z(t)}{\pi}(R_o^2 - R_i^2)^{-1}, \tag{15}$$

where R_o and R_i are the integration limits of the outer and inner diameter of the sample, respectively. The radius of the void space in the donut sample was measured after each rheological test to account for the effect of sample loading on R_i. The experimental reproducibility of measurements performed using the CP geometry was found to be $\pm 5\%$ for η^+ and $\pm 7\%$ for N_1^+.

C. Measurement of fiber orientation

The initial fiber orientation of the parallel plate and donut samples for PBT-30 was experimentally determined to aid in the analysis of the stress growth behavior. The initial orientation of the unmodified CP sample was believed to be the same as the donut sample as they were prepared in the same manner. Samples to be analyzed for their initial fiber orientation were loaded into their respective rheometer fixture at 260 °C to give the same shear history as the samples used for rheological measurements. Each sample was imaged perpendicular to the flow direction (x_2–x_3 plane). We define x_1 as the flow direction, x_2 as the direction of velocity gradient, and x_3 as the neutral direction. The samples were prepared to be imaged by embedding quartered sections in epoxy, sanding to a specific plane depth, and then polishing to a final abrasive particle size of 0.3 μm Al_2O_3 following standardized techniques [Sawyer and Grubb (1995)]. Extreme precaution was taken to ensure all sanding and polishing was performed parallel to the plane of interest. A schematic drawing of the polished planes and locations where the images were taken can be found in Fig. 3. To establish the average orientation through the sample, images were taken at three locations, at distances of 4.0, 6.25, and 8.5 mm from the outer edge denoted

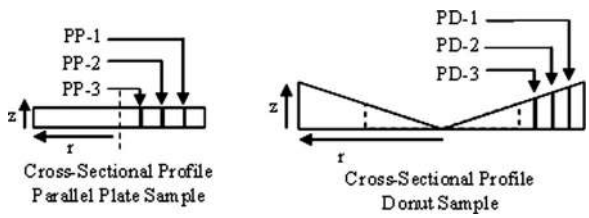

FIG. 3. Representative drawing of the cross-sectional profile of a parallel pate and donut sample. The confocal laser microscopy images were taken for the parallel plate sample at a distance of 4.0, 7.0, and 10.0 mm from the outer edge denoted by PP-1, PP-2, and PP-3, respectively. Similarly, the images were taken for the donut sample at a distance of 4.0, 6.25, and 8.5 mm from the outer edge denoted by PD-1, PD-2, and PD-3.

by PD-1, PD-2, and PD-3, respectively, for the donut sample and 4.0, 7.0, and 10.0 mm from the outer edge denoted by PP-1, PP-2, and PP-3, respectively, for the PP sample.

Images were taken using a Zeiss LSM 510 confocal laser scanning microscope fitted with a 40x water immersion objective lens and a laser excitation wavelength of 543 nm. The final image was 230×230 μm^2 with a resolution of 1024×1024 pixels. For each sample, sequential images were taken from the bottom to the top in the direction of the velocity gradient and at two planes of depth. The confocal laser is able to penetrate the sample surface and focus at various depths. This allowed for a full three-dimensional description of the fiber orientation and removed the ambiguity associated with reflection microscopy techniques such as the Leeds method [Hine *et al.* (1993)]. For the PBT-30, the maximum penetration was found to be 8 μm. In an image, the cross section of each fiber appears as circles or ellipse-like shapes. To process the image, the circumference of each fiber intersection was traced by hand to improve the contrast between the fibers and the matrix and converted to a binary image. A computer program was written combined with image analysis software in MATLAB that measured the position of center of mass, the major and minor axes, and local angle between the image axis and the major axis of the ellipse. The components of **u** for each fiber were determined from the elliptical "footprint" at two cross-sectional planes. A full description of this technique can be found elsewhere [Lee *et al.* (2002); Eberle *et al.* (2008, 2009a)].

With knowledge of the components of the vector **u** for each fiber, the tensor **A** was determined as a weighted sum of all fibers [Bay and Tucker (1992)],

$$A_{ij} = \frac{\Sigma (u_i u_j)_n F_n}{\Sigma F_n}, \quad F_n = \frac{M_n}{m_n}, \tag{16}$$

where F_n is a weighting function for the nth fiber and M_n and m_n are the major and minor axes of each fibers elliptical footprint, respectively. The weighting function is based on the probability of a two-dimensional plane intersecting a fiber. Meaning, a fiber aligned perpendicular to the plane is more likely to be severed than one aligned parallel. Using the weighting function, the larger the aspect ratio of the ellipse, the more that fiber is weighted. The reproducibility of A_{ij} component between different samples was found to be dependent on the magnitude of the A_{ij} component with the maximum error being $\pm 12.4\%$ for the component of smallest magnitude, the A_{22}.

IV. RESULTS AND DISCUSSION

In the subsequent subsections, we first present experimental results of the stress growth behavior measured using the PP geometry as a function of gap height. We then discuss the design of the donut shaped sample to maintain a sufficient gap to fiber length ratio. This is followed by a comparison of stress growth behavior measured using the PP geometry and the CP-D geometry. Finally, predictions of the Lipscomb model stress coupled with the Folgar–Tucker model for orientation are fit to the transient stress growth measurements. The effect of the initial conditions on the model predictions and the model parameters determined from fitting stress growth data measured using the PP geometry and the CP-D are discussed.

A. Effect of gap in PP geometry

Gap effects on the transient rheological behavior of suspensions containing short glass fibers have previously been reported in literature. In semidilute and concentrated suspensions, insufficient gap heights have been shown to suppress the overshoot behavior [Utracki (1991); Djalili-Moghaddam *et al.* (2004)]. For our work, it was crucial to deter-

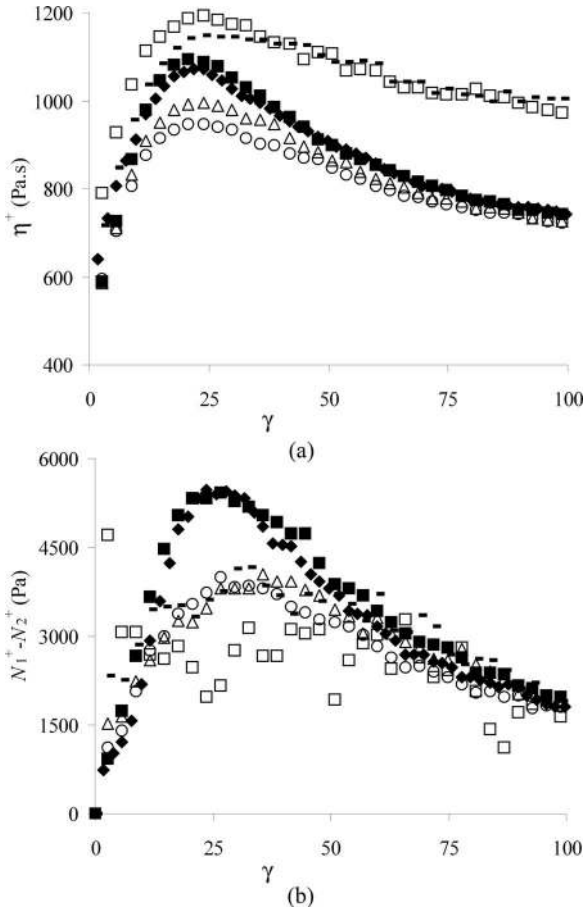

FIG. 4. The effect of the PP geometry gap height on the stress growth behavior of PBT-30 in startup of flow experiments at $\dot{\gamma}=1\ s^{-1}$. (a) η^+ vs strain and (b) N_1^+–N_2^+ vs strain. The various symbols relate to measurements performed at the different gap heights of 0.2 (□), 0.4 (–), 0.6 (△), 0.8 (○), 1.0 (■), and 1.2 mm (◆).

mine the dependence of the overshoot on rheometer gap height for two reasons. The first was to follow common procedures in literature to perform measurements using the PP geometry that were independent of gap height. The other reason was to determine the minimum gap height at which the measurements were independent of gap height to aid in the design of the donut sample. This was accomplished by performing startup of flow experiments on PBT-30 using various gaps in the PP geometry. The results can be seen in Figs. 4(a) and 4(b) for η^+ and N_1^+–N_2^+, respectively vs γ at $\dot{\gamma}_R=1\ s^{-1}$. For gaps that were roughly $\leq 2L_n$ (gaps: 0.2, 0.4, 0.6, and 0.8 mm), the rheological properties were highly dependent on the gap height. At the smallest gaps (gaps: 0.2 and 0.4), η^+ was enhanced and took a much longer time for the overshoot to approach a steady state, and N_1^+–N_2^+ was very "noisy" and suppressed compared to measurements at the other gaps. As a note, the measurements performed using gaps ≤ 0.6 mm were not reproducible within a reasonable experimental error and the plots in Figs. 4(a) and 4(b) are a representation only. As the gap was increased to 0.8 mm, the measurements of η^+ and N_1^+–N_2^+ became repeatable and developed a consistent overshoot. However, the overshoot remained gap dependent

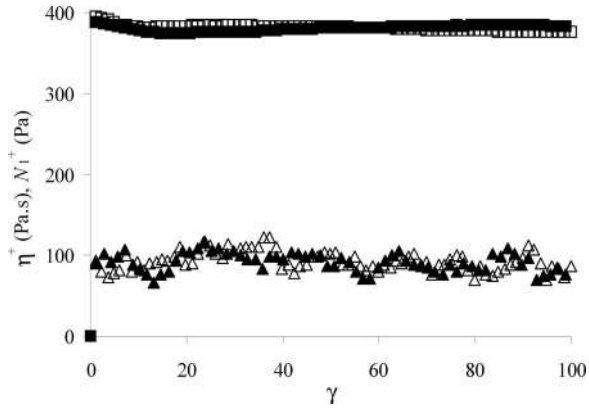

FIG. 5. The stress growth behavior of the neat PBT measured using the 50 mm CP geometry with an unmodified sample and with the CP-D. The symbols (□) and (■) represent η^+ and (△) and (▲) represent N_1^+ measured using the CP and CP-D, respectively. Measurements were performed at $\dot{\gamma}=1\ s^{-1}$.

until 1.0 mm which is $>2L_n$. For gaps 1.0 and 1.2 mm, η^+ exhibited an overshoot that was reproducible within relative error of the experiment $\pm 5\%$. As a result, all further experiments using the PP were performed at a gap of 1.0 mm.

B. Donut sample

In designing the donut sample, the purpose of the hole was to remove any the excessive fiber-boundary interaction at the center that could potentially affect the transient rheological behavior. The experiments discussed above, using the PP geometry with various gap heights, showed that for PBT-30 there was a negligible effect on the stress growth behavior when the gap was greater than twice the number average fiber length. The gap within the 50 mm CP fixture varied linearly from 2.51 mm at the outer edge to 0.05 mm at the center. As a result, a 25.4 mm diameter hole was drilled through the center of the molded CP samples, which ensured the gap was always greater than $2L_n$. Figure 5 shows the stress growth behavior of the neat PBT measured using the 50 mm CP geometry combined with an unmodified sample and with the donut sample. After correcting for the void area at the center of the donut samples using Eqs. (14) and (15), the measured stresses were found to be within experimental error when compared to measurements performed with unmodified samples.

C. Stress growth

We now consider the effect of fiber concentration on the stress growth behavior measured using the CP-D and PP geometries. The shear stress growth coefficient η^+ vs strain as a function of fiber concentration measured using the PP geometry and using the CP-D can be seen in Figs. 6(a) and 6(b), respectively. Up to 15 wt %, the maximum value of η^+ measured using both techniques is relatively similar, within experimental error. However, for higher concentrations, the magnitude of η^+ measured using the PP geometry is always much larger, with the greatest difference being at the largest concentration of fiber, 30 wt %.

The normal stress difference growth, $N_1^+ - N_2^+$ (measured using the PP fixture), N_1^+ (measured using the CP geometry) vs strain as a function of concentration can be seen in Figs. 7(a) and 7(b), respectively. For up to 8.42 wt %, the maximum values of $N_1^+ - N_2^+$ and

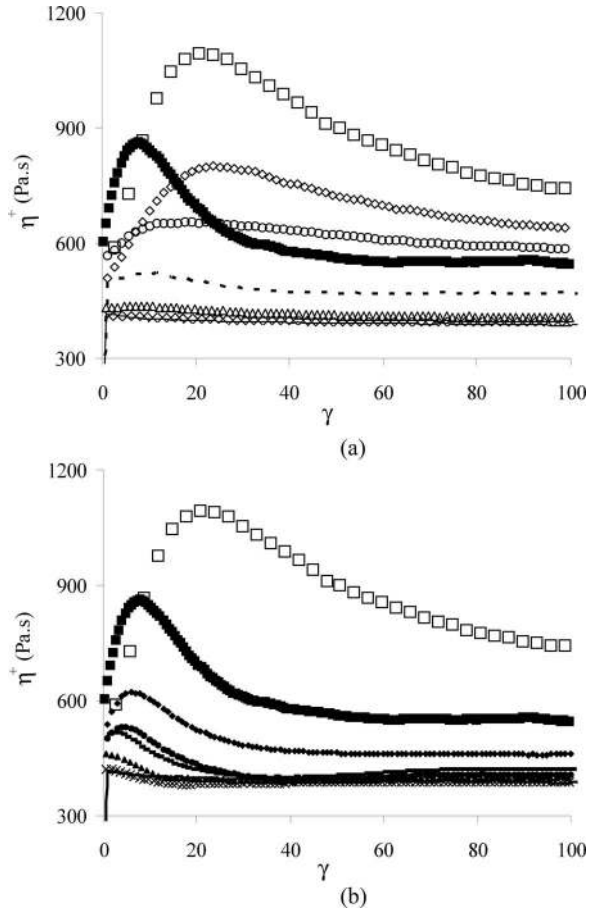

FIG. 6. η^+ vs strain as a function of concentration at $\dot{\gamma}=\dot{\gamma}_R=1\ \ s^{-1}$. (a) Measurements performed using the PP geometry. The symbols (×), (△), (−), (○), (◇), and (□) represent fiber weight percent 4.07, 8.42, 15, 20, 25, and 30. The symbol (■) represents η^+ of PBT-30 measured using the CP-D for comparison. (b) Measurements performed using the CP-D. The symbols (×), (▲), (−), (●), (◆), and (■) represent fiber weight percent 4.07, 8.42, 15, 20, 25, and 30. The symbol (□) represents the stress growth of PBT-30 measured using the PP geometry for comparison. The line shows the neat PBT for comparison in both graphs.

N_1^+ are within experimental error of each other. However, the difference drastically increases with concentration varying in magnitude from 56% for 15 wt % to 214% for 30 wt % fiber when compared to the CP-D measurements.

In this work, we directly compare N_1^+–N_2^+ measured using the PP geometry with N_1^+ measured using the CP. For viscoelastic fluids, it is typically found that $-N_2<10\%N_1$, where N_1 and N_2 relate the steady state first and second normal stress differences [Bird *et al.* (1987)]. The published data relating to the magnitude of N_2 in glass fiber suspensions are limited, but what is available suggests the same trend applies, $-N_2<10\%N_1$ [Chan *et al.* (1978); Zirnsak *et al.* (1994)]. Simulations of the rheological material functions show the magnitude of N_2^+ is small compared to N_1^+. In addition, at low concentrations ($\leq$8.42 wt%), N_1^+–N_2^+ and N_1^+ are of similar magnitude. As a result, we assume that N_2^+ in the concentrated systems is small compared to N_1^+ and cannot account for the large difference in the direct comparison of N_1^+–N_2^+ and N_1^+.

As discussed above, the greatest difference between the measured material functions is

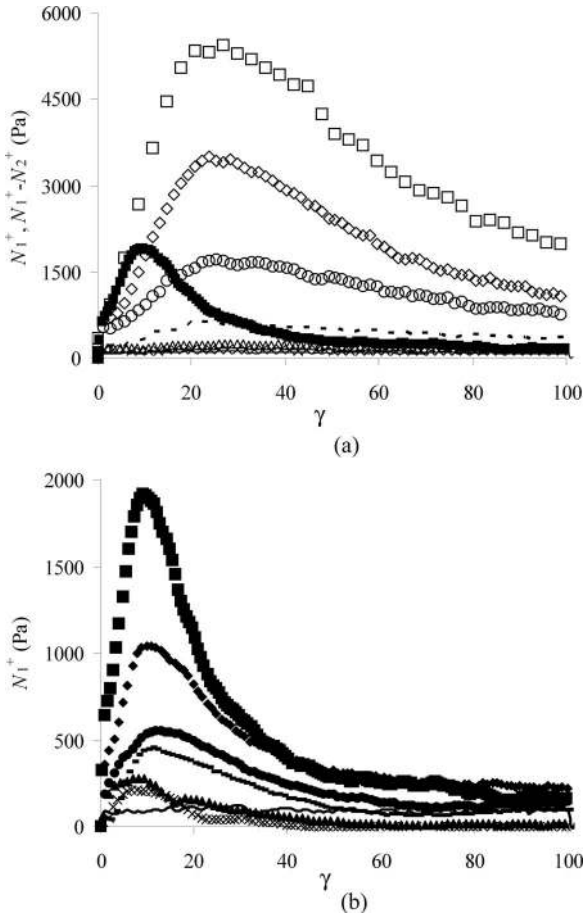

FIG. 7. N_1^+ and N_1^+–N_2^+ vs strain at $\dot{\gamma}=\dot{\gamma}_R=1\ s^{-1}$. (a) Measurements performed using the PP geometry. The symbols (×), (△), (−), (○), (◇), and (□) represent fiber weight percent 4.07, 8.42, 15, 20, 25, and 30. The symbol (■) represents the N_1^+ of PBT-30 measured using the CP-D for comparison. (b) Measurements performed using the CP-D. The symbols (×), (▲), (−), (●), (◆), and (■) represent fiber weight percent 4.07, 8.42, 15, 20, 25, and 30. The line shows the neat PBT for comparison in both graphs.

found to be at the highest concentration. In addition, the highest concentration is the one of greatest practical interest and, as a result, the rest of the paper focuses on the stress growth behavior of PBT-30. The stress growth behavior of PBT-30 in startup of flow measured using the PP geometry at $\dot{\gamma}_R=1\ s^{-1}$ and CP geometry at $\dot{\gamma}=1\ s^{-1}$ can be seen in Figs. 8(a) and 8(b). In Fig. 8(a) η^+ vs strain is shown for measurements performed with the PP fixture, the CP fixture with unmodified sample, and the CP fixture combined with the donut sample CP-D. First we compare the differences between η^+ measured with the CP fixtures using the unmodified sample and the donut sample. The value of the peak of the η^+ overshoot is within experimental error between the two measurements. However, η^+ decays toward a lower steady state value in the case of the donut sample. This behavior is attributed to the small gaps at the center of the plate inducing excessive fiber-boundary interaction and interfering with the evolution of the fiber microstructure in the unmodified sample.

We now compare the stress growth behavior of PBT-30 measured using the CP-D with that measured using the PP geometry. η^+ measured using the CP-D and the PP fixtures

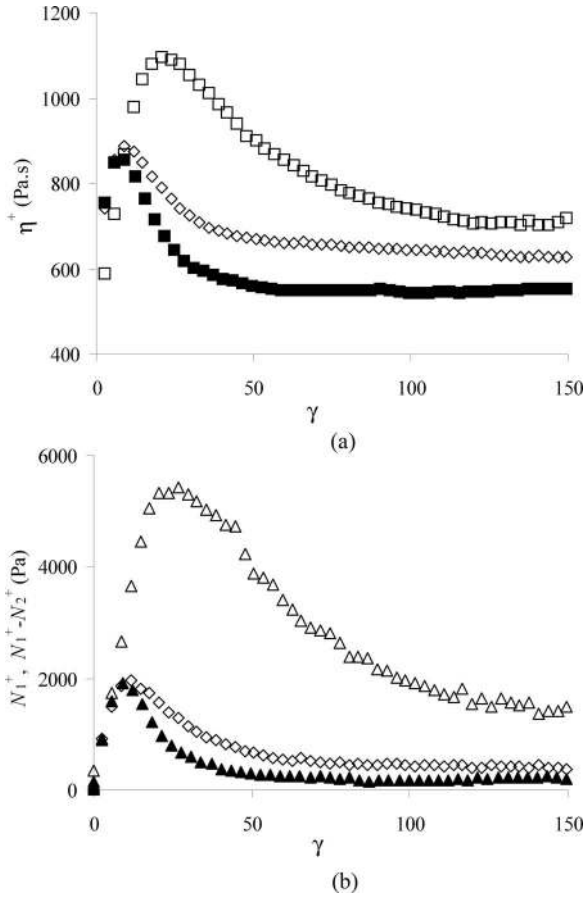

FIG. 8. Stress growth vs strain in startup of flow measurements for PBT-30 at $\dot{\gamma}=\dot{\gamma}_R=1\ s^{-1}$. (a) η^+ measured using the PP (□), the CP with unmodified sample (◇), and the CP-D (■). (b) N_1^+–N_2^+, N_1^+ measured using the PP (△), the CP with unmodified sample (⌑), and the CP-D (▲).

can be seen in Fig. 8(a). The magnitude of the overshoot for η^+ is much greater in the measurement using the PP geometry. In addition, the onset of steady state occurs at roughly 150 strain units, which is in contrast to the roughly 50 strain units at which the CP-D measurement approaches a steady state. In Fig. 8(b) N_1^+ is shown measured using the CP fixture for both the modified sample and the donut sample and N_1^+–N_2^+ measured using the PP fixture. First we compare N_1^+ measured using the CP fixture for both the unmodified sample and the CP-D. The overshoot of N_1^+ measured with the donut sample decays at a faster rate than that measured using the unmodified sample, which results in a smaller overshoot width. Again, we attribute this behavior to the small gaps at the center of the plate inducing excessive fiber-boundary interaction, interfering with the evolution of the fiber microstructure in the unmodified sample. The differences between the measurements performed using the PP fixture and the CP-D are much greater. The peak value of the overshoot measured using the PP geometry is more than three times that measured using the CP-D. In addition, the onset of steady state occurs at roughly 150 strain units for N_1^+–N_2^+ in contrast to the roughly 50 strain units for N_1^+.

The same differences in the stress growth behavior measured using the PP geometry and the CP-D also occur at different shear rates. Figures 9(a) and 9(b) show the stress

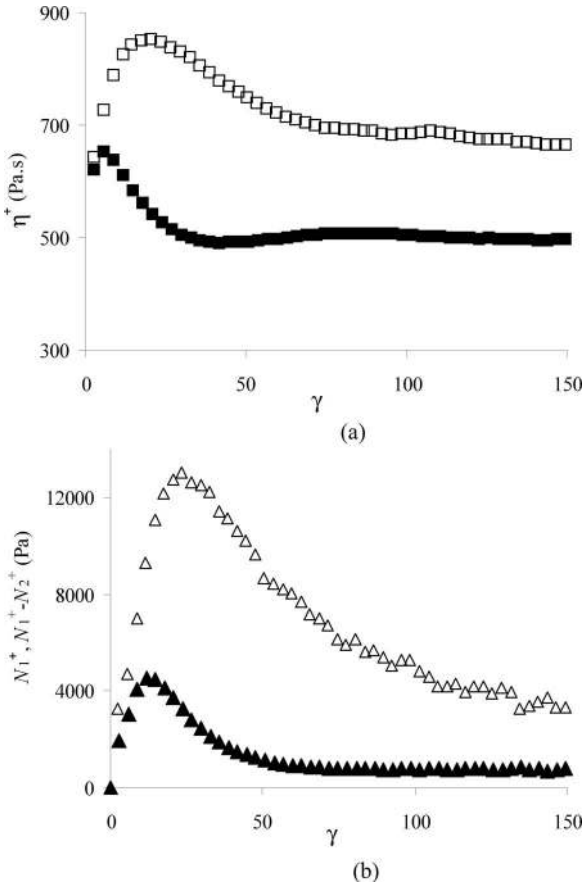

FIG. 9. Stress growth vs strain in startup of flow measurements for PBT-30 at $\dot{\gamma}=\dot{\gamma}_R=4\ s^{-1}$. (a) η^+ measured using the PP (□) and the CP-D (■). (b) N_1^+–N_2^+, N_1^+ measured using the PP (△), and the CP-D (▲).

growth behavior in startup of flow measurements for PBT-30 at $\dot{\gamma}=4\ s^{-1}$ for η^+ and N_1^+–N_2^+, N_1^+ vs strain, respectively. In both Figs. 9(a) and 9(b), the stresses measured using the CP-D are smaller in magnitude and approach a steady state at a smaller strain than that measured using the PP geometry.

As a result of the inhomogeneous velocity field, one would expect the width of the overshoot to be greater for the measurement performed using the PP fixture. However, the difference in magnitude is not as intuitive. One plausible hypothesis as to why the transient stresses measured using the PP geometry are greater than those measured using the CP-D can be supported by looking at suspension theory. In the dilute suspension theory, the motion of a fiber, in terms of spherical angles θ and φ, is governed by Eqs. (4) and (5), respectively. Both θ and φ are functions of time and shear rate. In Fig. 10, θ and φ vs time are depicted using initial conditions $\theta_o=60°$ and $\varphi_o=175°$ for various shear rates, $\dot{\gamma}=1$, 0.2, and 0.1 s^{-1}. Fibers subject to higher shear rates rotate faster than those at lower shear rates. Moses *et al.* (2001) confirmed Jeffery's analysis for a dilute suspension of nylon fibers in a Newtonian suspending medium. In concentrated suspensions where the proximity of a neighboring fiber is on the order of the fiber diameter, the inhomogeneous velocity field imposed by the PP fixture could induce a high degree of direct fiber contact. As a result, the stresses measured using the PP geometry could be an inaccurate repre-

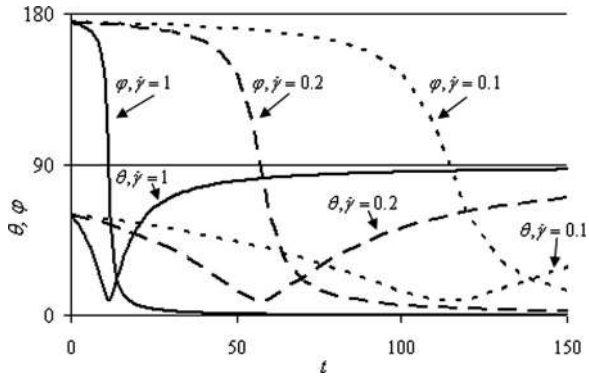

FIG. 10. Spherical angles θ and φ representing the reorientation of a fiber subject to simple shear flow vs time as predicted by Eqs. (4) and (5) for various shear rates, $\dot{\gamma}$=1, 0.2, and 0.1 s^{-1}. The initial conditions were φ_o=175°, θ_o=60°.

sentation of the stress growth behavior that arises from direct particle-particle contact induced by the inhomogeneous velocity field. If this is correct then fitting theory to measurements performed using the PP geometry would also lead to erroneous model parameters.

D. Simulations

In this subsection, we discuss the model predictions of the Lipscomb model for stress combined with the Folgar–Tucker model for orientation. The goals of this section are twofold. The first is to show that the transient model predictions are highly dependent on the initial fiber orientation. The second is to show that different model parameters may be obtained by fitting stresses measured in either the CP-D or the PP geometry.

For Eqs. (6) and (8)–(11), the fourth-order orientation tensor $\mathbf{A_4}$ was expressed in terms of $\mathbf{A}$ using the quadratic closure approximation, $\mathbf{A_4}=\mathbf{AA}$ [Doi and Edwards (1988)]. It is well known that the model predictions, and therefore, the parameters determined by fitting are highly dependent on the closure approximation. In this case, the quadratic closure was chosen because it allowed for relatively good agreement between the general characteristics of the predictions and the transient stresses. Eberle *et al.* (2009b) showed in detail how one can fit material parameters fiber-suspension theory using more a more complex closure approximation.

Equation (6), governing the time rate of change in the fiber orientation, was solved numerically using Gears implicit predictor-corrector method at a time step of 0.01 s. The results were confirmed to be independent of the time step by comparing the predictions at a time step of 0.001 s with those at 0.01 s. Initial conditions, which are crucial to the transient stress growth behavior, are discussed later. To solve for the material functions η^{PP} and N_1^{PP}–N_2^{PP}, Eqs. (10) and (11) were integrated using the trapezoid rule at each strain. The model parameter N was obtained by fitting the overshoot maximum of η^{CP} and η^{PP} to the peak of the η^+ overshoot measured using the CP-D and PP geometries, respectively. C_I was determined by fitting N_1^{CP} and N_1^{PP}–N_2^{PP} to the onset of the steady state plateau of N_1^+ and N_1^+–N_2^+, respectively. Because N and C_I were only fit to a portion of the stress growth curve, subsequently, we compare model predictions of η^{CP}, η^{PP}, N_1^{CP}, and N_1^{PP}–N_2^{PP} using the fitted parameters to the experimental data. The suspending medium viscosity was measured and determined to be η_s=372 Pa s.

TABLE I. The initial fiber orientation represented through the components of the orientation order parameter tensor **A**.

	A_{11}	A_{22}	A_{33}	A_{12}	A_{13}	A_{23}
PD-average	0.4371	0.0377	0.5252	0.0777	0.0604	0.0314
PP-average	0.4811	0.0618	0.4570	0.0950	−0.0241	−0.0280

It has been shown that model parameters for a given fluid may possibly be obtained by fitting suspension theory predictions to stress growth measurements [Sepehr *et al.* (2004a, 2004b)]. In the previous section, we showed that there is a large difference between the stress growth measurements performed using the CP-D and the PP geometries. The objective of the following subsection is to show that different material parameters can be obtained depending on the initial conditions used in the model predictions and which measurement the model is fit to, i.e., measurements performed using the CP-D and the PP geometries.

In the literature, it is commonly assumed that the fiber orientation is initially random [Ramazani *et al.* (2001); Sepehr *et al.* (2004a, 2004b)]. However, we find that the initial orientation is closer to a planar orientation with the majority of the fibers aligned in the x_1 and x_3 directions. The average fiber orientation data for the donut and the PP sample are reported in Table I. The A_{22} component for the PP sample was higher on average than for the donut sample. The large A_{11}, A_{33}, and small A_{22} components are believed to be a result of the sample deformation history, i.e., sample formation using compression molding.

The effect of initial conditions on the predictions of Eqs. (6), (8), and (9) fit to the stress growth data for PBT-30 measured using the CP-D at $\dot{\gamma}=1\ \mathrm{s}^{-1}$ can be seen in Fig. 11. The fit model parameters using the experimentally determined initial conditions were found to be $N=104$ and $C_I=0.000\,01$, and for the random initial conditions $N=14$, $C_I=0.000\,4$. First, there is almost an order of magnitude difference in the value of N and C_I

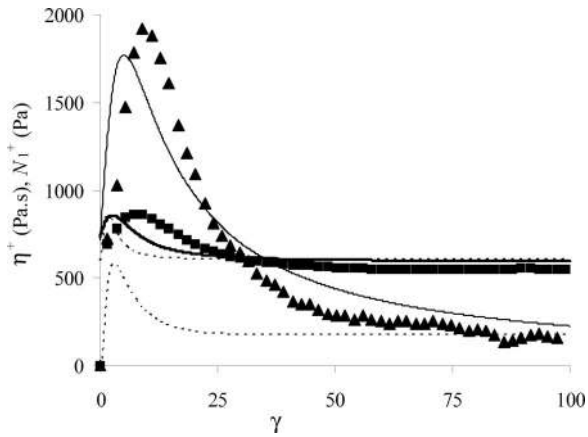

FIG. 11. Effect of initial conditions on the model fit to the experimentally determined η^+ (■) and N_1^+ (▲) for PBT-30 measured using the CP-D at $\dot{\gamma}=1\ \mathrm{s}^{-1}$. The line and bold line represent η^{CP} or Eqs. (6) and (8) for the random and experimentally determined initial conditions, respectively. The symbols (−) and (—) represent N^{CP} or Eqs. (6) and (9) for the random and experimentally determined initial conditions, respectively. Model parameters determined by fitting using the random initial conditions were $N=14$, $C_I=0.000\,4$, and using the experimentally determined initial conditions were $N=104$ and $C_I=0.000\,01$.

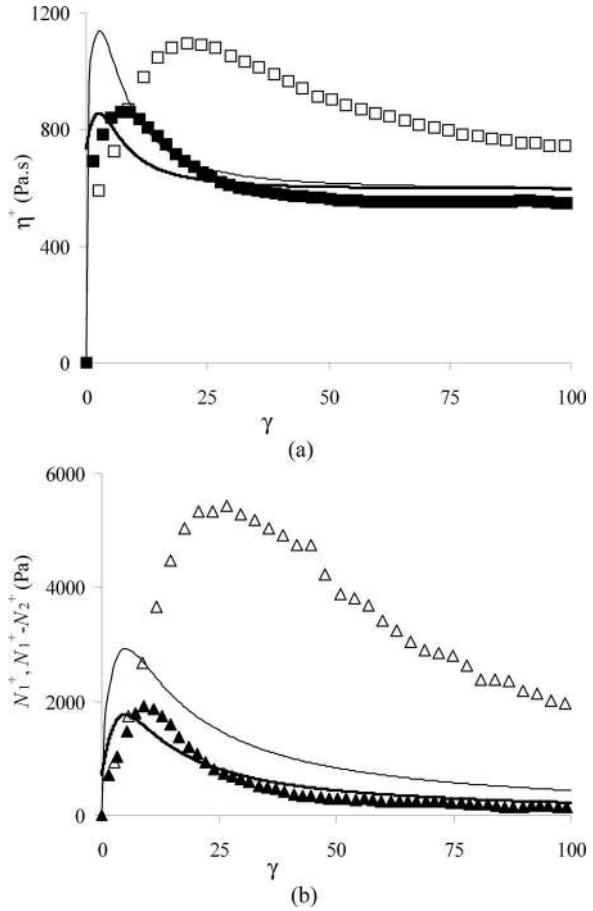

FIG. 12. Stress growth data and model predictions in startup of flow measurements for PBT-30 at $\dot{\gamma}=\dot{\gamma}_R=1\ s^{-1}$. (a) η^{PP} (line) fit to η^+ measured using the PP geometry (□); η^{CP} (bold line) fit to η^+ measured using the CP-D (■). (b) Predicted N_1^{PP}–N_2^{PP} and N_1^{CP} and experimentally determined N_1^+–N_2^+ and N_1^+ measured using the PP (△) and the CP-D (▲), respectively. For all predictions, $\eta_s=372$ Pa s and $C_I=0.000\,01$. For η^{CP} and N_1^{CP} $N=104$ and η^{PP} and N_1^{PP}–N_2^{PP} $N=136.6$.

determined using the different initial conditions. Second, there are a number of differences between the predictions. With the experimentally determined initial conditions, the prediction of N_1^{CP} is relatively good. The peak value of N_1^{CP} is within 7% of the measured peak value of N_1^+. Also, the width of the overshoot is of similar magnitude. However, the peak values of the η^+ and N_1^+ overshoot occur at a larger strain than the predicted η^{CP} and N_1^{CP}. This is in sharp contrast to the predictions using the random initial conditions. Using the random initial conditions, there is roughly a 71% difference between the predictions of the peak values of N_1^{CP} and the measured N_1^+. Also, the predictions of the width of the overshoot of η^{CP} and N_1^{CP} are much smaller than those of η^+ and N_1^+.

In Figs. 12(a) and 12(b), the experimental data and model predictions of the stress growth functions for a homogeneous (CP geometry) and inhomogeneous (PP geometry) velocity field denoted by superscripts CP and PP, respectively, at similar shear rates of $\dot{\gamma}=\dot{\gamma}_R=1\ s^{-1}$ are shown. In Fig. 12(a) the predictions of η^{CP} and η^{PP} compared to η^+ measured using the CP-D and PP geometries are shown. Both η^{CP} and η^{PP} were unable to predict the width of the experimentally observed overshoot, but the predictions for η^{CP}

were closer. For η^{CP} and η^{PP}, the initial conditions were taken to be those found experimentally, and the best fit value of N was determined to be $N=104$ and $N=136.6$, respectively. This is a difference of roughly 30% in the value of N. In Fig. 12(b) the experimental values of N_1^+, $N_1^+-N_2^+$, and predicted values of N_1^{CP}, $N_1^{PP}-N_2^{PP}$ vs strain are shown. The predictions for N_1^{CP} were very close to the measured values when the magnitude of the overshoot maximum is compared. This is in sharp contrast to the predictions of $N_1^{PP}-N_2^{PP}$ compared to the measured values. The magnitude of the overshoot maximum for $N_1^{PP}-N_2^{PP}$ is over 50% less than the measured value. For both N_1^{CP} and $N_1^{PP}-N_2^{PP}$, the models were unable to predict the width of the overshoot but the predictions were better for the case of N_1^{CP}. For both N_1^{CP} and $N_1^{PP}-N_2^{PP}$, the best fit value of C_I was determined to be $C_I=0.000\ 01$.

V. CONCLUSIONS

We propose that the inhomogeneous velocity field imposed by a PP geometry leads to radially dependent periods of rotation for the fiber inducing excessive fiber-fiber interaction when the orientation is evolving with time. This exaggerates the magnitude of the stress growth functions and possibly the width of the overshoot. If this hypothesis is correct, PP fixtures should not be used to quantitatively characterize the stress growth functions of concentrated suspensions containing glass fibers. In addition, fitting model parameters to stress growth functions of concentrated suspensions containing high aspect ratio particles measured with a PP geometry would give inaccurate values. Furthermore, obtaining accurate values of parameters in the theory for stress and orientation requires an accurate knowledge of the initial orientation of the fibers which can be a function of the sample preparation conditions.

We suggest an approach to characterize the rheological behavior of suspensions containing short glass fibers that uses a donut shaped sample in a CP geometry. We believe that measurements performed using this approach give an accurate representation of the stress response to deformation in simple shear flow. However, these results are given in light of the effect that the curvilinear stream lines might have on the rheological behavior. Future experiments using a sliding plate rheometer, which imposes rectilinear streamlines with a homogeneous velocity field, will be used to confirm our findings.

ACKNOWLEDGMENTS

The financial support for this work from the National Science Foundation and Department of Energy through Grant No. DMI-0521918 is gratefully acknowledged. We thank GE Plastics for supplying the materials used in this work.

References

Advani, S. G., and E. M. Sozer, *Process Modeling in Composites Manufacturing* (Marcel Dekker, New York, 2003).

Advani, S. G., and C. L. Tucker, "The use of tensors to describe and predict fiber orientation in short fiber composites," J. Rheol. **31**, 751–784 (1987).

Barbosa, S. E., and M. A. Bibbo, "Fiber motion and the rheology of suspensions with uniform fiber orientation," J. Polym. Sci., Part B: Polym. Phys. **38**, 1788–1799 (2000).

Bay, R. S., and C. L. Tucker, "Stereological measurement and error estimates for three dimensional fibre orientation," Polym. Eng. Sci. **32**, 240–253 (1992).

Bird, R. B., R. C. Armstrong, and O. Hassager, *Dynamics of Polymeric Liquids* (Wiley, New York, 1987).

Blakeney, W. R., "Viscosity of suspensions of straight rigid rods," J. Colloid Interface Sci. **22**, 324–330 (1966).

Botelho, G., A. Queiros, S. Liberal, and P. Gijsman, "Studies on thermal and thermo-oxidative degradation of poly(ehtylene terephthalate) and poly(butylene terephthalate)," Polym. Degrad. Stab. **74**, 39–48 (2001).

Chan, Y., J. L. White, and Y. Oyanagi, "A fundamental study of the rheological properties of glass-fiber-reinforced polyethylene and polystyrene melts," J. Rheol. **22**, 507–524 (1978).

Dinh, S. M., and R. C. Armstrong, "A rheological equation of state for semiconcentrated fiber suspensions," J. Rheol. **28**, 207–227 (1984).

Djalili-Moghaddam, M., R. Ebrahimzadeh, and S. Toll, "Study of geometry effects in torsional rheometry of fiber suspensions," Rheol. Acta **44**, 29–37 (2004).

Doi, M., and S. F. Edwards, *The Theory of Polymer Dynamics* (Oxford University Press, New York, 1988).

Eberle, A. P. R., "The dynamic behavior of a concentrated composite fluid containing non-Brownian glass fibers in rheometrical flows," Ph.D. thesis, Virginia Tech, 2008.

Eberle, A. P. R., D. Baird, and P. Wapperom, "Rheology of non-Newtonian fluids containing glass fibers: A review of experimental literature," Ind. Eng. Chem. Res. **47**, 3470–3488 (2008).

Eberle, A. P. R., G. M. Vélez-García, D. G. Baird, and P. Wapperom, "Fiber orientation kinetics of a concentrated short glass fiber suspension in startup of simple shear flow," J. Non-Newtonian Fluid Mech. (submitted).

Eberle, A. P. R., D. G. Baird, P. Wapperom, and G. M. Vélez-García, "Using transient shear rheology to determine material parameters in fiber suspension theory," J. Rheol. **53**, 685–705 (2009b).

Einstein, A., "A new determination of molecular dimensions," Ann. Phys. **19**, 289–306 (1906).

Folgar, F. P., and C. L. Tucker, "Orientation behavior of fibers in concentrated suspensions," J. Reinf. Plast. Compos. **3**, 98–119 (1984).

Ganani, E., and R. L. Powell, "Suspensions of rodlike particles: Literature review and data correlations," J. Compos. Mater. **19**, 194 (1985).

Giesekus, H., "Stromungen mit konstantem Geschwindigkeitsgradienten und die Bewegung von darin suspendierten Teilchen. Teil I: Raumliche Stromungen," Rheol. Acta **2**, 101–112 (1962a).

Giesekus, H., "Stromungen mit konstantem Geschwindigkeitsgradienten und die Bewegung von darin suspendierten Teilchen. Teil II: Ebene Stromungen undeine experimentelle Anordnung zuihrer Realisierung," Rheol. Acta **2**, 112–122 (1962b).

Hand, G. L., "A theory of dilute suspensions," Arch. Ration. Mech. Anal. **7**, 81–86 (1961).

Hine, P. J., N. Davidson, R. A. Duckett, and I. M. Ward, "Measuring the fibre orientation and modeling the elastic properties of injection-moulded long-glass-fibre-reinforced nylon," Compos. Sci. Technol. **53**, 125–131 (1993).

Iso, Y., D. L. Koch, and C. Cohen, "Orientation in simple shear flow of semi-dilute fiber suspensions. 1. Weakly elastic fluids," J. Non-Newtonian Fluid Mech. **62**, 115–134 (1996).

Jeffery, G. B., "The motion of ellipsoidal particles immersed in a viscous fluid," Proc. R. Soc. London, Ser. A **102**, 161–179 (1922).

Larson, R. G., *The Strucuture and Rheology of Complex Fluids* (Oxford University Press, New York, 1999).

Laun, H. M., "Orientation effects and rheology of short glass fiber-reinforced thermoplastics," Colloid Polym. Sci. **262**, 257–269 (1984).

Lee, Y., S. Lee, J. Youn, K. Chung, and T. Kang, "Characterization of fiber orientation in short fiber reinforced composites with an image processing technique," Mater. Res. Innovations **6**, 65–72 (2002).

Lipscomb, G. G., M. M. Denn, D. U. Hur, and D. V. Boger, "The flow of fiber suspensions in complex geometries," J. Non-Newtonian Fluid Mech. **26**, 297–325 (1988).

Macosko, C. W., *Rheology Principles, Measurements, and Applications* (Wiley-VCH, New York, 1994).

Moses, K. B., S. G. Advani, and A. Reinhardt, "Investigation of fiber motion near solid boundaries in simple shear flow," Rheol. Acta **40**, 296–306 (2001).

Phan-Thien, N., and A. L. Graham, "A new constitutive model for fiber suspensions," Rheol. Acta **30**, 44–57 (1991).

Powell, R. L., "Rheology of suspensions of rodlike particles," J. Stat. Phys. **62**, 1073–1091 (1990).

Ramazani, A., A. Ait-Kadi, and M. Grmela, "Rheology of fiber suspensions in viscoelastic media: Experiments and model predictions," J. Rheol. **45**, 945–962 (2001).

Sawyer, L. C., and D. Grubb, *Polymer Microscopy* (Springer, New York, 1995).

Sepehr, M., G. Ausias, and P. J. Carreau, "Rheological properties of short fiber filled polypropylene in transient shear flow," J. Non-Newtonian Fluid Mech. **123**, 19–32 (2004a).

Sepehr, M., P. J. Carreau, M. Grmela, G. Ausias, and P. G. Lafleur, "Comparison of rheological properties of fiber suspensions with model predictions," J. Polym. Eng. **24**, 579–610 (2004b).

Sepehr, M., P. J. Carreau, M. Moan, and G. Ausias, "Rheological properties of short fiber model suspensions," J. Rheol. **48**, 1023–1048 (2004c).

Shaqfeh, E. S. G., and G. H. Fredrickson, "The hydrodynamic stress in a suspension of rods," Phys. Fluids A **2**, 7–25 (1990).

Utracki, L. A., *Two-Phase Polymer Systems* (Oxford University Press, New York, 1991).

Zirnsak, M. A., D. U. Hur, and D. V. Boger, "Normal stresses in fibre suspensions," J. Non-Newtonian Fluid Mech. **54**, 153–193 (1994).